

## Chemically ordered decahedral FePt nanocrystals observed by electron microscopy

Zi-An Li,<sup>1</sup> M. Spasova,<sup>1</sup> Q. M. Ramasse,<sup>2</sup> M. E. Gruner,<sup>1</sup> C. Kisielowski,<sup>3</sup> and M. Farle<sup>1,\*</sup>

<sup>1</sup>*Faculty of Physics and Center for Nanointegration Duisburg-Essen (CeNIDE), University Duisburg-Essen, D-47048 Duisburg, Germany*

<sup>2</sup>*SuperSTEM Laboratory, STFC Daresbury Campus, Keckwick Lane, Daresbury WA44AD, United Kingdom*

<sup>3</sup>*National Center for Electron Microscopy, Lawrence Berkeley National Laboratory, University of California, Berkeley, California 94720, USA*

(Received 5 August 2013; revised manuscript received 31 March 2014; published 24 April 2014)

The crystal structure of FePt nanoparticles of mean size of 6 nm produced by gas-phase condensation is characterized using a combination of high-resolution transmission electron microscopy (HRTEM) and high-angle annular dark field (HAADF) imaging in scanning transmission electron microscopy (STEM). These FePt nanoparticles are found to be chemically ordered, decahedral shaped, and Pt enriched at the surfaces. The experimentally determined crystallographic lattice constants and distribution of Fe and Pt atoms are compared with *first-principles* calculations of ordered decahedral FePt nanoparticles to confirm the discovery of a unique decahedral structure with Fe/Pt ordering and Pt surface segregation.

DOI: [10.1103/PhysRevB.89.161406](https://doi.org/10.1103/PhysRevB.89.161406)

PACS number(s): 61.46.Df, 64.75.Jk, 68.37.Og, 75.75.Fk

Understanding the equilibrium shape and morphology of nanoparticles has been a challenge for more than a century since the first analysis of morphology and facet formation by Wulff [1]. The experimentally demonstrated coexistence of various structural motifs implies the presence of a complex energy landscape with different local minima for the nucleation of small clusters and the subsequent shellwise growth into nanoparticles (NPs). For example, in the same size range and for identical synthesis conditions, it is possible to find both regular crystal NPs and multiply twinned particles (MTPs), as first observed by Ino [2] and Allpress [3]. Decahedra and icosahedra are specific forms of MTPs which have been the subject of intensive studies, and substantial information about their properties, structure, defects, and elastic deformations has been gathered to date through both experiment and theory, as seen in recent reviews [4,5] and references therein.

While the atomistic structure of elementary metallic MTPs such as Au NPs [4] has been fully characterized, the understanding of compound and multicomponent alloy MTPs is still challenging owing to additional energetic complexities imposed by the homogeneity or local inhomogeneity of their compositions, by their distinct chemistry, and by order-disorder phenomena. Little is known [6] as to whether and how (i) alloying affects the formation of MTPs, (ii) element segregation affects the MTPs formation, and (iii) structurally or chemically driven transitions, such as the disorder-order transition in an alloy, can occur in nanoparticles, which are susceptible to energetically large, non-bulk-like surface effects.

We have been investigating a prototype system consisting of gas-phase-synthesized Fe-Pt nanoparticles that exhibit rich structural and magnetic properties [7,8]. Depending on the kinetic synthesis conditions, the FePt alloy crystallizes either in the chemically disordered face-centered cubic structure (A1 phase) or in a chemically ordered structure with face-centered tetragonal coordination (L1<sub>0</sub> phase). Regardless of the synthesis route, FePt MTPs often coexist with regular single crystals [9,10]. Recent experiments [11–13] and calculations [14,15] suggest that FePt NPs show Pt segregation towards their surfaces (and possibly also at internal interfaces [16]). Such

“self-assembled” ferromagnetic particles with a Pt-enriched surface are thus environmentally stable against oxidation [12]. Additionally, the surface Pt acts as a catalyst yielding the possibility to manipulate noninvasively the magnetically active and catalytic particles using magnetic gradient fields [13,17,18].

Theoretical studies have been undertaken to look into the energetics of ordering, twinning, and element segregation in bimetallic 3d-5d transition metal alloys [19,20]. Large scale first-principles calculations predict that small FePt NPs (3 nm or less) thermodynamically favor the formation of chemically ordered FePt MTPs [19]. This is attributed to the efficient strain release due to the formation of twin boundaries in alloyed MTPs. Recent results on single-crystalline 3 nm NPs produced by organometallic synthesis confirm this theoretical finding [21]. Also, the synthesis of ordered decahedral clusters of CoPt and FePt (2 to 5 nm) showing no preferential surface segregation of one element was recently demonstrated using a cluster source technique with subsequent annealing in a carbon matrix [22].

In this Rapid Communication we confirm the theoretically predicted and experimentally observed formation of chemically ordered 6 nm FePt decahedra using high-resolution electron microscopy techniques. Detailed lattice parameters and local chemical compositions of the 6 nm particles are evaluated from HRTEM and HAADF lattice images with atomic resolution. This grants direct experimental insight into the formation of alloyed nanoparticle systems and reveals a complex interplay of element ordering, alloying, segregation, and strain.

The atomistic structure of single-element decahedral particles [Fig. 1(a)] has been debated mainly in terms of two competing models [23]: (i) the so called homogenous strain model, wherein a body-centered orthorhombic (BCO) unit cell can be constructed within each structural subunit [24]; and (ii) the inhomogeneous strain model, in which a slightly distorted BCO unit cell due to wedge disclination [25] is formed. The orthorhombic lattice constants of each subunit are defined for both models in Figs. 1(b) and 1(c), respectively. Note that these two models are based on purely geometrical considerations, packing identical spheres without taking into account any element specificity or the effects of twinning

\*Corresponding author: michael.farle@uni-due.de

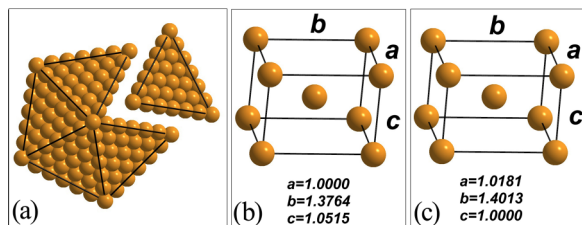


FIG. 1. (Color online) Schematics of decahedral packing with identical spheres. (a) Regular decahedron viewed along its fivefold axis. One of the five tetrahedral subunits is detached for clarity. (b) Body-centered orthorhombic unit cell in the decahedral subunit, as per Bagley's homogeneous strain model. (c) Body-centered orthorhombic unit cell in the decahedral subunit, as per de Wit's inhomogeneous strain model. Reduced lattice parameters are indicated in the figures.

boundaries. As pointed out recently for the case of decahedral Au NPs, such a simple-minded model may not even be adequate for the description of single-element decahedra [23,26].

FePt particles were prepared by gas-phase condensation and annealed in vacuum in the gas phase as described in previous publications [27]. Details are given in the Supplementary Material [28]. The lattice constants of ordered decahedral FePt found within the sample were measured using atomically resolved HRTEM and HAADF lattice images. The contrast of HAADF images arises from electrons scattered to high angles, mainly through thermal diffuse scattering. In our experimental conditions, the HAADF intensity scales to a good approximation with the square of the atomic number  $Z$  of the observed atomic column and is hence often referred to as  $Z$  contrast. Figure 2(a) shows an atomically resolved HAADF image of a typical chemically ordered Marks-type decahedral FePt NP with reentrant (111) facets. A striking feature is the shellwise oscillatory contrast variations, which we attribute to the chemically ordered state of Fe and Pt: brighter atomic columns are identified as heavy Pt shells ( $Z = 78$ ), while dimmer columns in adjacent shells correspond to Fe ( $Z = 26$ ). This contrast is most evident when the atomic columns of the NP are perfectly aligned with the incident beam, providing ideal channeling conditions.

Although the particle [Fig. 2(a)] appears slightly tilted from its ideal fivefold axis, the structural domain pointing towards 3 o'clock is still in excellent channeling conditions and illustrates well the oscillating contrast across the alternating Fe and Pt layers. The very bright contrast of the central column suggests that it is mainly comprised of Pt atoms. In the outer shells of the particle (which contain fewer atoms per column), the nearly identical contrast for adjacent shells [denoted by white arrows in Fig. 2(a)] indicates Pt-enriched and Pt-terminated surface shells. This Pt enrichment at the surface can be ascribed to the tendency of the Pt atoms to segregate to the surface during particle formation through the in-flight annealing process [11–13].

To verify the above  $Z$ -contrast analysis, HAADF image simulations using a multislice algorithm were performed with the QSTEM software [29]. More details of the atomic model and image simulation parameters are given in the Supplementary Material [28]. Figure 2(b) shows the HAADF

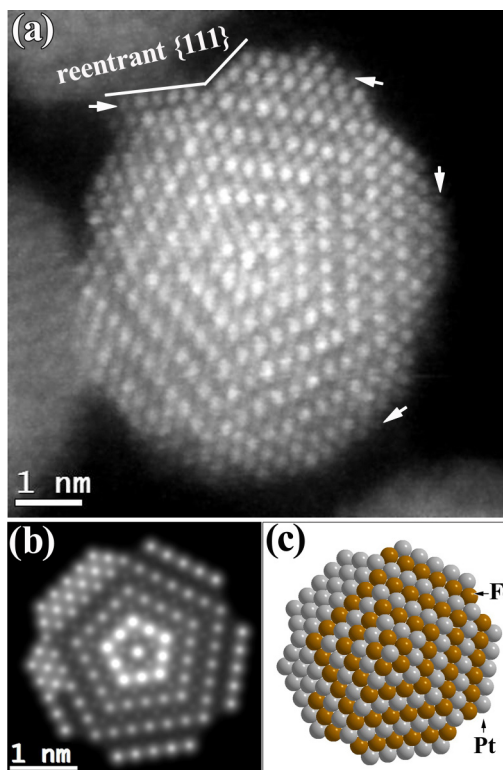


FIG. 2. (Color online) (a) Experimental high-resolution HAADF (Z-contrast) image of a chemically ordered decahedral FePt NP. Brighter spots correspond to heavy Pt atomic columns ( $Z = 78$ ), while less bright spots correspond to Fe columns ( $Z = 26$ ). The white arrows indicate Pt-enriched surfaces which contain only few atoms in the column. (b) HAADF simulation of an ordered decahedral FePt NP according to the atomic model of ordered decahedral FePt shown in (c).

image simulation of a chemically ordered decahedral FePt NP assuming additional Pt segregation and Pt termination at the surface [Fig. 2(c)]. The bright simulated contrast at the surface is more prominent than in the experimental observations. As the simulations assume the presence of a pure Pt termination, this most likely points to a nonfully saturated Pt surface in the experiment. Nevertheless, the enhanced contrast at the surface provides strong qualitative evidence that the outer layers of the particles are Pt enriched in comparison to the core. Unfortunately, an atomically resolved chemical map with EELS or EDS which could unambiguously confirm the Pt-enriched surface layer could not be recorded in these experiments.

HRTEM, for which, unlike in HAADF, the image formation relies on phase contrast, was also used to characterize the FePt NPs structure at atomic resolution. Figure 3(a) shows a typical HRTEM lattice image of another chemically ordered decahedral FePt nanoparticle. The pentagonal symmetry of the image readily identifies it as a projection of a decahedral particle along its fivefold axis [Fig. 3(a)]. In the digital diffractogram of the particle [Fig. 3(b)] the appearance of (001) fcc forbidden spots is the characteristic signature of Fe/Pt ordering. The decahedral particle is comprised of five structural domains of nearly identical size. The particle core

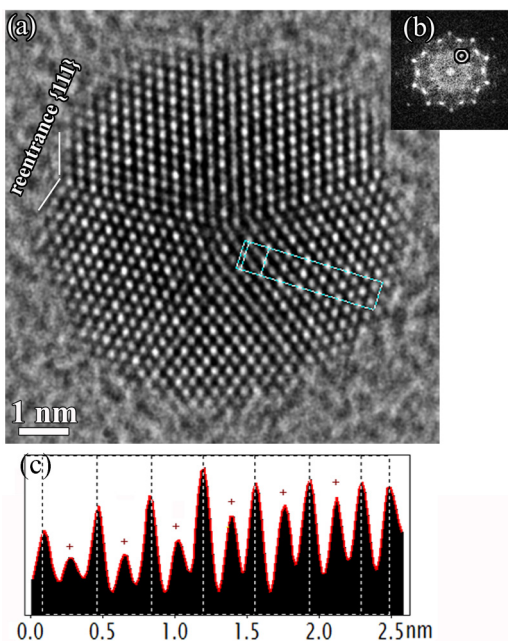


FIG. 3. (Color online) (a) Experimental HRTEM image of chemically ordered Marks-decahedral FePt NP. One set of reentrant (111) planes is indicated. (b) Digital diffractogram of image (a). The (001) fcc forbidden spots (white circle) appear only in the chemically ordered state of Pt/Fe. Note that the Miller indices take the notation of fcc structure. (c) Intensity profile showing shellwise oscillatory contrast as extracted from the region framed by the blue-dash box in (a).

is at the geometric center where the five twin planes intersect. The interior of the five domains are free of planar defects such as stacking faults or dislocations, as are the twin boundaries. As in the particle imaged by HAADF in Fig. 2(a), reentrant (111) facets are observed at the particle surface. Figure 3(c) shows an intensity profile extracted from the region indicated in Fig. 3(a), revealing oscillatory contrast variations. These contrast variations, though depending on defocus due to the phase contrast nature of HRTEM images, are closely related to the ordered state of Fe and Pt. Decahedral particles of disordered FePt or of pure elementary Au do not exhibit such oscillatory contrast variations regardless of focus conditions [30]. To verify the origin of these contrast variations, extensive HRTEM image simulations using experimental microscope parameters were performed on various decahedral motifs with ordered and disordered structures as well as with pure Au NPs (see Supplementary Material [28]). These image simulations unambiguously confirm that the Fe and Pt ordering is responsible for the observed oscillatory contrast variations.

Quantitative planar (2D) atomic displacements and strain distribution can be extracted from the atomic resolution images. To accurately measure the atomic column positions, an exit-wave reconstruction approach is used [31]. The reconstructed phase images present minimal imaging artifacts, no delocalization effect, and an enhanced signal-to-noise ratio. This allows us to precisely correlate the phase contrast maxima with atomic column positions [32]. Figure 4(a) shows the phase image of an ordered decahedral FePt NP reconstructed

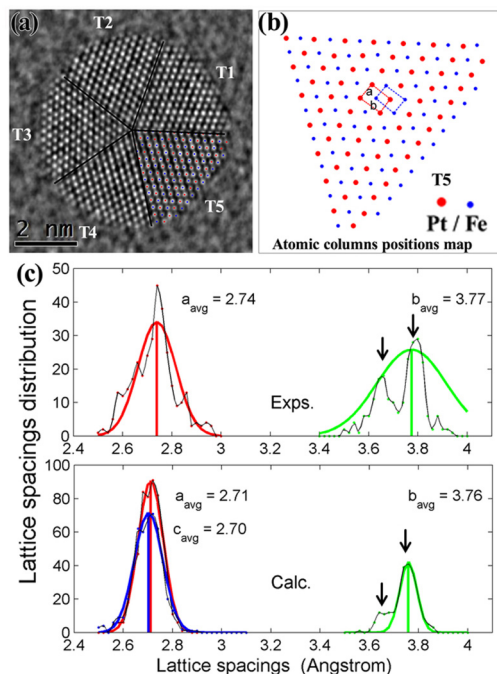


FIG. 4. (Color online) (a) Phase image reconstructed from a focus series of 20 lattice images. Five twin boundaries are outlined by black solid lines and their twinned units are indicated by  $T_n$  ( $n = 1-5$ ). (b) Atom columns positions map for T5. The orthorhombic unit cell parameters  $a$  and  $b$  are indicated. (c) Experimental (upper panel) and calculated (lower panel) distributions of lattice spacings. Gaussian fits for distributions of lattice constants  $a$  (red),  $b$  (green), and  $c$  (blue, calculated only) are provided as a guide to the eye. Average lattice constants are given in both cases. The arrows indicate the peaks of a bimodal distribution of lattice spacing  $b$ .

from 20 lattice images acquired at different focus values. The five twinned subunits are denoted as “ $T_n$ ” ( $n = 1-5$ ): the extracted atom column positions are overlaid on T5 and also enlarged in Fig. 4(b) for clarity. The extracted atomic column position maps allow us to determine the orthorhombic lattice constants  $a$  and  $b$ , as defined in the decahedral models in Figs. 1(b) and 1(c) and on the map of Fig. 4(b). The measured lattice spacing distribution is given in the upper panel of Fig. 4(c), yielding mean values of  $a = 0.274$  and  $b = 0.377 \pm 0.005$  nm (see Supplementary Material for details of the analysis [28]). Unfortunately, the inherent limitation of 2D projection imaging of a 3D object in this microscopy study prevents the evaluation of the lattice constant  $c$  (along the fivefold axis). For completeness we note that recent progress in 3D atomic resolution imaging has enabled the direct visualization of atomic twin boundaries and detailed dislocation structures in decahedral Pt nanocrystals [33].

The relatively broad distribution of lattice spacings in Fig. 4(c) is partly attributed to the fact that the measurements were performed on projection images in which several factors complicate the lattice determination (see measurement errors discussion in the Supplementary Material [28]). To substantiate this aspect independently we compare our experimental lattice values with parameter-free first-principles calculations (see Supplementary Material [28]). The lattice spacings for different crystallographic directions of an ordered decahedral

3 nm FePt cluster (923 atoms) are shown in the lower panel of Fig. 4(c). The mean values are  $a_{\text{calc}} = 0.271$  nm,  $b_{\text{calc}} = 0.376$  nm, and  $c_{\text{calc}} = 0.270$  nm in very good agreement with our experimental findings. For a better understanding of this distortion from bulk we note that for perfect fcc tetrahedral subunits the angle between adjacent (111) faces is  $70.53^\circ$ , which results in a total  $7.35^\circ$  solid-angle deficiency when adding five subunits to form a decahedron. Interestingly, we can therefore conclude from the existence in practice of such decahedral binary particles that the overall binding energy for this size range of particles is minimized when the unit cells of each subunit adopt a body-centered orthorhombic lattice, as shown in Figs. 1(b) and 1(c). This distortion from the bulk equilibrium compensates the angle deficiency completely. By geometrical arguments the  $b/a$  ratio of the body-centered orthorhombic lattice is fixed at  $\cotan(36^\circ) \approx 1.376$  for a perfect decahedral symmetry. Our experimentally measured mean lattice values lead to an excellent agreement, as we find  $b/a = 1.376$ , whereas the calculated  $T = 0$  K value  $b_{\text{calc}}/a_{\text{calc}} = 1.387$  is larger by about 1%. We note that Crangle *et al.* [34] reported lattice parameters  $a = c = 0.2761$  nm,  $b = 0.3735$  nm for decahedral FePt, corresponding to a lower  $b/a = 1.353$ . This measurement however was carried out on a “bulk” sample, not on a single near-ideal decahedral NP as in our case. Deviation from the ideal ratio of 1.376 in such overall lattice analysis could suggest that “real” nanoparticles contain defects or are intrinsically strained [23]. Additionally, the lattice parameter  $b$  seems to follow a bimodal distribution in both experiment and theory, as indicated by arrows in Fig. 4(c). While this bimodal behavior could reflect a difference in lattice spacing between the surface and the core of the particle, we can clearly exclude this interpretation: Strain maps extracted from the calculated positions of Fe and Pt showed a random distribution of these two values of  $b$  throughout the particle (see [28]). We therefore tentatively attribute this distribution of lattice spacings to the complexity of site-dependent nearest-neighbor coordination due to the competition of Fe/Pt ordering and Pt segregation in the alloyed FePt NPs. This inhomogeneous lattice relaxation found in our experiment and calculations emphasizes that the nature of crystal structure formation in alloyed decahedral particles is more complex than can be properly described by previously proposed simple geometrical models.

Our size-dependent first-principles comparison of different morphologies [19] suggest that for FePt the energetic crossover between multiply twinned particles, which are preferred at smaller diameters, and single-crystalline morphologies should be expected around 4 nm. Model investigations based on Lennard-Jones potentials demonstrate that multiply twinned particles are additionally supported by vibrational entropy [35], so these morphologies might be found stable at finite temperature also at larger sizes. This is evidenced by the presence of FePt icosahedra of 4 nm [11] and FePt decahedra of 6 nm in our experiments. In addition, our larger particles are in the shape of a Marks-type rather than Ino-type decahedron, which results in the efficient release of internal strain by creating additional (111) surfaces, which possess a significantly lower surface energy in the case of a pure Pt termination (see Ref. 10 in [28]). While our previous experimental results show that icosahedral 4 nm FePt NPs with Pt-enriched surfaces were produced by only slightly different synthesis conditions

(pressure of 0.5 mbar) in the gas-phase synthesis, our present TEM data show that Pt-enriched icosahedra coexist with chemically ordered decahedra in the size range of 5–7 nm produced at a pressure of 1 mbar.

As already pointed out by Tournus *et al.* [22] our structural and compositional findings may help to explain the previously reported suppression of the high magnetocrystalline anisotropy in chemically ordered FePt nanoparticles. We recall that a lattice distortion of less than 2% of a ferromagnet with cubic (fcc or bcc) structure may enhance its magnetocrystalline anisotropy density by 2 orders of magnitude as, for example, evidenced in face-centered tetragonal Ni films on Cu(100) [36]. Previous results on icosahedral particles along with the present report suggest quite significant inhomogeneous lattice distortions (e.g., at the surface, near twin boundaries) and a Pt concentration gradient—that is, locally varying degrees of chemical order—within the particle. Both effects [36,37] contribute to strongly varying local magnetic anisotropies within the particle [19]. Furthermore, in the ordered decahedral arrangement, the easy axes of magnetization in the five individual domains compete, and thus the single-domain ferromagnetic state enforced by exchange interaction results in largely compromised hard-magnetic properties [38], as previously suggested by Tournus *et al.* [22]. In view of these results a consistent model emerges explaining the strong decrease of the large  $L1_0$  magnetocrystalline anisotropy energy density of uncapped FePt particles (see, for example, [9,19,39]) with particle size.

In summary, using two independent types of atomically resolved imaging techniques, we confirmed the existence of chemically ordered decahedral FePt nanoparticles and found their lattice spacings and composition in good quantitative agreement with the atomic positions obtained by state-of-the-art first-principles calculations. For sizes up to 6 nm we find a coexistence of multiply twinned and single-crystalline alloyed particles, as expected from first-principles calculations and thermodynamic considerations. In addition, the structural and compositional results provide direct evidence for a Pt surface segregation. Our observation of large (6 nm) ordered *bimetallic* decahedral particles may contribute to a better understanding of the formation and the crystallography and morphology of alloyed multiply twinned particles. Finally, we note that the observed formation of well-ordered decahedral FePt particles with multiple local magnetic anisotropy axes and likely Pt surface segregation provides further evidence that uncapped, ideally  $L1_0$ -ordered FePt NPs in the size range below 4 nm, may not be thermodynamically stable [8,22].

We thank Dr. C. Y. Song and Dipl. Ing. H. Zähres for technical support and Dr. O. Dmitrieva for part of the sample preparations. The work was supported by the Deutsche Forschungsgemeinschaft, SFB 445 and the EU consortium REFreePerMag. Electron microscopy was performed at National Center of Electron Microscopy at Berkeley which is supported by the Office of Science, Office of Basic Energy Sciences of the US Department of Energy under Contract No. DE-AC02-05CH11231. Computing resources were kindly provided by the John von Neumann Institute for Computing (NIC) on the IBM Blue Gene Supercomputing system at Forschungszentrum Jülich.

- [1] G. Wulff, *Z. Krystal. Miner.* **34**, 449 (1901).
- [2] S. Ino, *J. Phys. Soc. Jpn.* **21**, 346 (1966).
- [3] J. G. Allpress and J. V. Sanders, *Surf. Sci.* **7**, 1 (1967).
- [4] L. D. Marks, *Rep. Prog. Phys.* **57**, 603 (1994).
- [5] V. G. Gryaznov, J. Heydenreich, A. M. Kaprelov, S. A. Nepijko, A. E. Romanov, and J. Urban, *Cryst. Res. Technol.* **34**, 1091 (1999).
- [6] E. Ringe, R. P. V. Duyne, and L. D. Marks, *Nano. Lett.* **11**, 3399 (2011).
- [7] J. Lyubina, B. Rellinghaus, O. Gutfleisch, and M. Albrecht, *Handbook of Magnetic Materials*, Vol. 19, edited by K. H. J. Buschow (Elsevier North-Holland, Amsterdam, 2011), Chap. 5, pp. 291–407.
- [8] C. Antoniak *et al.*, *Nat. Commun.* **2**, 528 (2011).
- [9] B. Rellinghaus *et al.*, *J. Magn. Magn. Mater* **266**, 142 (2003).
- [10] S. Stappert, B. Rellinghaus, M. Acet, and E. Wassermann, *J. Crystal Growth* **252**, 440 (2003).
- [11] R. M. Wang, O. Dmitrieva, M. Farle, G. Dumpich, H. Q. Ye, H. Poppa, R. Kilaas, and C. Kisielowski, *Phys. Rev. Lett.* **100**, 017205 (2008).
- [12] L. Y. Han, U. Wiedwald, B. Kuerbanjiang, and P. Ziemann, *Nanotechnology* **20**, 285706 (2009).
- [13] R. M. Wang *et al.*, *J. Phys. Chem. C* **113**, 4395 (2009).
- [14] B. Yang, M. Asta, O. N. Mryasov, T. J. Klemmer, and R. W. Chantrell, *Scr. Mater.* **53**, 417 (2005).
- [15] M. Müller and K. Albe, *Phys. Rev. B* **72**, 094203 (2005).
- [16] K. L. Torres and G. B. Thopson, *Ultramicroscopy* **109**, 606 (2009).
- [17] P. Strasser *et al.*, *Nat. Chem.* **2**, 454 (2010).
- [18] R. Ferrando, A. Fortunelli, and R. L. Johnston, *Phys. Chem. Chem. Phys.* **10**, 640 (2008).
- [19] M. E. Gruner, G. Rollmann, P. Entel, and M. Farle, *Phys. Rev. Lett.* **100**, 087203 (2008).
- [20] M. E. Gruner and P. Entel, *Int. J. Quantum Chem.* **112**, 277 (2012).
- [21] M. Delalande, M. J. F. Guinel, L. F. Allard, A. Dellatre, R. Le Bris, Y. Samson, P. Bayle-Guillemand, and P. Reiss, *J. Phys. Chem. C* **116**, 6866 (2012).
- [22] F. Tournus, K. Sato, T. Epicier, T. J. Konno, and V. Dupuis, *Phys. Rev. Lett.* **110**, 055501 (2013).
- [23] C. L. Johnson, E. Snoeck, M. Ezcurdia, B. Rodriguez-Gonzalez, I. Pastoriza-Santos, L. M. Liz-Marzan, and M. J. Hyetch, *Nat. Mater.* **7**, 120 (2008).
- [24] B. G. Bagley, *Nature (London)* **208**, 674 (1965).
- [25] R. de Wit, *J. Phys. C: Solid State Phys.* **5**, 529 (1972).
- [26] H. Hofmeister, *Cryst. Res. Technol.* **33**, 3 (1998).
- [27] O. Dmitrieva *et al.*, *Phys. Rev. B* **76**, 064414 (2007).
- [28] See Supplemental Material at <http://link.aps.org/supplemental/10.1103/PhysRevB.89.161406> for the sample preparation, the details of HRTEM and HAADF microscopic experiments and image simulation, and the details of lattice evaluations using experimental images.
- [29] C. Koch, Ph.D. thesis, Arizona State University, USA, 2002.
- [30] Z. R. Dai, S. Sun, and Z. L. Wang, *Surf. Sci.* **505**, 325 (2002).
- [31] R. W. Gerchberg and W. O. Saxton, *Optik (Stuttgart)* **35**, 237 (1972).
- [32] C. Kisielowski, C. J. D. Hetherington, Y. Wang, R. Kilaas, M. O'Keefe, and A. Thust, *Ultramicroscopy* **89**, 243 (2001).
- [33] C. C. Chen, C. Zhu, E. R. White, C. Y. Chiu, M. C. Scott, B. C. Regan, L. D. Marks, Y. Huang, and J. W. Miao, *Nature (London)* **496**, 74 (2013).
- [34] J. Crangle and J. A. Shaw, *Philos Mag* **7**, 207 (1962).
- [35] J. P. K. Doye and F. Calvo, *Phys. Rev. Lett.* **86**, 3570 (2001).
- [36] M. Farle, *Rep. Prog. Phys.* **61**, 755 (1998).
- [37] J. B. Staunton, S. Ostanin, S. S. A. Razee, B. Gyroffly, L. Szunyogh, B. Ginatempo, and E. Bruno, *J. Phys: Condens. Matter.* **16**, S5623 (2004).
- [38] K. Zhang, X. Hu, L. Xie, J. Yuan, J. Zhu, and D. Wei, *IEEE Trans. Magn.* **45**, 4427 (2009).
- [39] C. Antoniak *et al.*, *Phys. Rev. Lett.* **97**, 117201 (2006).